

We are IntechOpen, the world's leading publisher of Open Access books Built by scientists, for scientists

6,900

Open access books available

186,000

International authors and editors

200M

Downloads

Our authors are among the

154

Countries delivered to

TOP 1%

most cited scientists

12.2%

Contributors from top 500 universities



WEB OF SCIENCE™

Selection of our books indexed in the Book Citation Index
in Web of Science™ Core Collection (BKCI)

Interested in publishing with us?
Contact book.department@intechopen.com

Numbers displayed above are based on latest data collected.
For more information visit www.intechopen.com



XAFS Measurement System in the Soft X-Ray Region for Various Sample Conditions and Multipurpose Measurements

Koji Nakanishi and Toshiaki Ohta
*The SR Center, Ritsumeikan University,
Japan*

1. Introduction

An X-ray absorption fine structure (XAFS) spectroscopy is a powerful and useful technique to probe the local electronic structure and the local atomic structure around an absorbing atom in an unknown material [Stöhr, 1996, Ohta, 2002]. A highly bright X-ray source, synchrotron radiation (SR) is usually used for XAFS measurements to obtain reliable spectra, even for elements of very low content in a sample.

For visible/ultraviolet (UV) and infrared absorption spectroscopies, the transmission mode is generally used, where incident and transmitted photon intensities are monitored. This is also the most fundamental technique for XAFS measurements in the hard X-ray region. However, it is hard to apply it in the soft X-ray region because of very low transmission. Instead, other techniques equivalent to the transmission mode have been developed; total/partial electron yield (EY) and fluorescent yield (FY) modes. The former is a widely adopted mode in the soft X-ray region, where the yield of Auger electrons and/or secondary electrons is proportional to the X-ray absorption coefficient. Since the electron escape depth is very short, the EY mode is surface sensitive. The latter is useful for XAFS measurement of heavy elements of low concentration in the hard X-ray region, and it is also useful as a bulk sensitive method in the soft X-ray region, although the probability of radiative decay is much smaller than that of Auger decay. It is often the case that an appropriate mode is chosen for sample conditions.

We have developed a practical and useful XAFS measurement system in the soft X-ray region applicable for various sample conditions and multipurpose measurements. In this system, it is possible to measure not only solid samples (such as powder, grain, sheet and thin film samples) but also liquid and gel samples. It is also applicable to in-situ measurements of anaerobic samples. In addition, it provides us some information of depth profiles with combined use of the EY and FY modes.

2. XAFS measurement system in the soft X-ray region

The XAFS measurement system is an assembly of several components; a soft X-ray beamline, sample chambers, detection systems, and a sample transfer system. Details of each component are described follow.

2.1 Soft X-ray double-crystal monochromator beamline

For a beamline below 1000 eV, a grating monochromator is generally used, while a crystal monochromator is advantageous above 1000 eV, since several high quality crystals are available which have proper lattice spacings. For XAFS measurements in the higher-energy soft X-ray region (above 1000 eV), the double-crystal monochromator (DCM) beamline (BL-10) was constructed in the SR center, Ritsumeikan University in Japan [Iwasaki, et al., 1998, Handa, et al., 1999]. Then BL-10 has been developed and upgraded, and many measurements have been performed (see Fig. 1) [Nakanishi & Ohta, 2009]. It consists of a 5.1 μm thick Be foil, a Ni-coated Si toroidal mirror, a Golovchenko-type DCM [Golovchenko et al., 1981], an I_0 monitor made of either Cu or Al mesh, a high-vacuum (HV) sample chamber kept below 2×10^{-5} Pa, an atmospheric-pressure (AP) sample chamber, and some masks and slits (see Fig. 2 (a)). The Be foil and the toroidal mirror at the front line are cooled by water in order to reduce a heat load by direct irradiation of white X-rays. The Be foil functions to cut visible and vacuum-ultra-violet photons which cause a background of an XAFS spectrum. The SR beam with 6 mrad (horizontal) and 2 mrad (vertical) is deflected upward by 1.4° and focused at the sample position in the AP sample chamber about 9 m apart from the source point with the 1:1 geometry by the toroidal mirror. The beam shapes and sizes are in good agreement with those simulated by the ray trace analysis, as shown in Fig. 2 (b)-(d). The available photon energy covers a range from about 1000 to 4500 eV by choosing a pair of monochromatizing crystals, such as beryl(10-10), KTP(011), InSb(111), Ge(111), Si(111) and Si(220) whose 2d lattice spacings are 1.5965, 1.0954, 0.7481, 0.6532, 0.6270 and 0.3840 nm, respectively. The incident angle to the monochromatizing crystal, θ is read in high accuracy with an angle encoder. The photon energy is determined with the 2d lattice spacing of a monochromatizing crystal and the incident angle using Bragg's law. Several masks and slits were inserted to minimize stray lights.

2.2 Tandem-type high-vacuum and atmospheric-pressure sample chambers

It is challenging to obtain reliable spectra from highly reactive compounds. In the soft X-ray region, XAFS spectra are usually measured in vacuum because of the low transmittance of X-rays in air (see Fig. 3). A vacuum environment is also necessary to measure reliable spectra from highly hygroscopic samples. In contrast, some compounds change their structures in vacuum. A typical case is hydrated compounds, in which hydrated water molecules are easily desorbed in vacuum. In addition, liquid solutions or nano-particles suspended in liquid cannot be introduced in vacuum without a special cell. For such samples, XAFS measurements in AP are necessary.

Another compact AP sample chamber, made of an ICF70 six-way cross nipple, was installed at the downstream of the HV sample chamber (see Fig. 2, 4 (a)). Two chambers are separated by a thin Be window, which should be tolerable against 1 atm pressure difference and whose thickness should be as thin as possible to minimize the intensity loss. The beam size at the sample position in the HV sample chamber is about 2.5 mm (vertical) \times 6 mm (horizontal) (not focused), while that in the AP chamber is about 2 mm (vertical) \times 5 mm (horizontal) (focused). Thus, we chose the diameter of 10 mm and thickness of 15 μm , respectively (see Fig. 4 (b)). It has been working without any trouble for more than one year [Nakanishi et al., 2010].

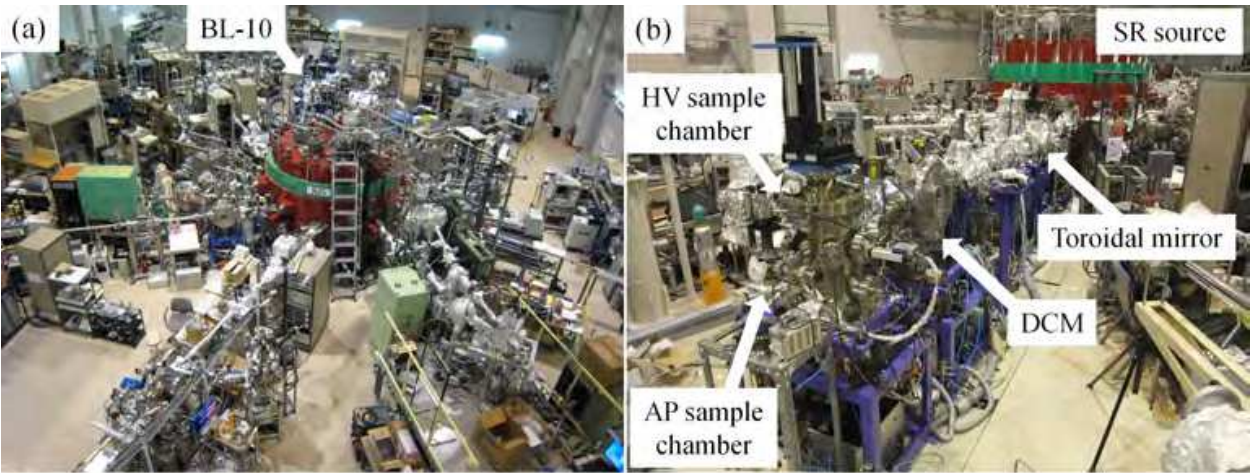


Fig. 1. (a) Bird-eye view of the SR center, Ritsumeikan University; (b) Photo of BL-10. Fourteen beamlines have been installed in the center; five beamlines for XAFS, three for X-ray lithography, three for photoelectron spectroscopy, and one for soft X-ray microscopy, infrared microscopy and X-ray reflectivity.

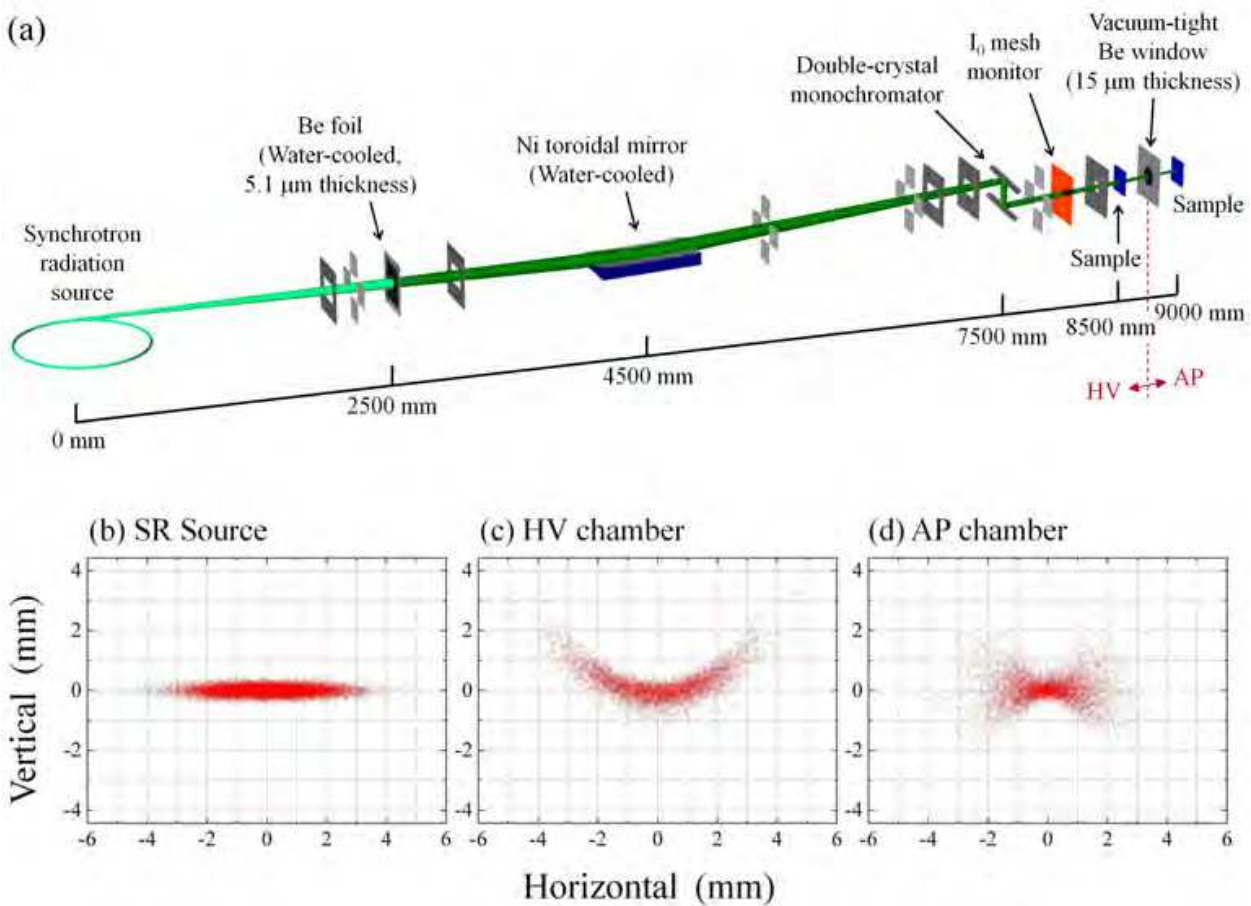


Fig. 2. (a) Schematic configuration of BL-10, and simulated X-ray beam profiles at (b) the source point; (c) the sample position of the HV chamber and (d) the sample position of AP chamber. The SR ray-tracing program “SHADOW” [Lai & Cerrina, 1986, Welna et al., 1996] was used for the simulations.

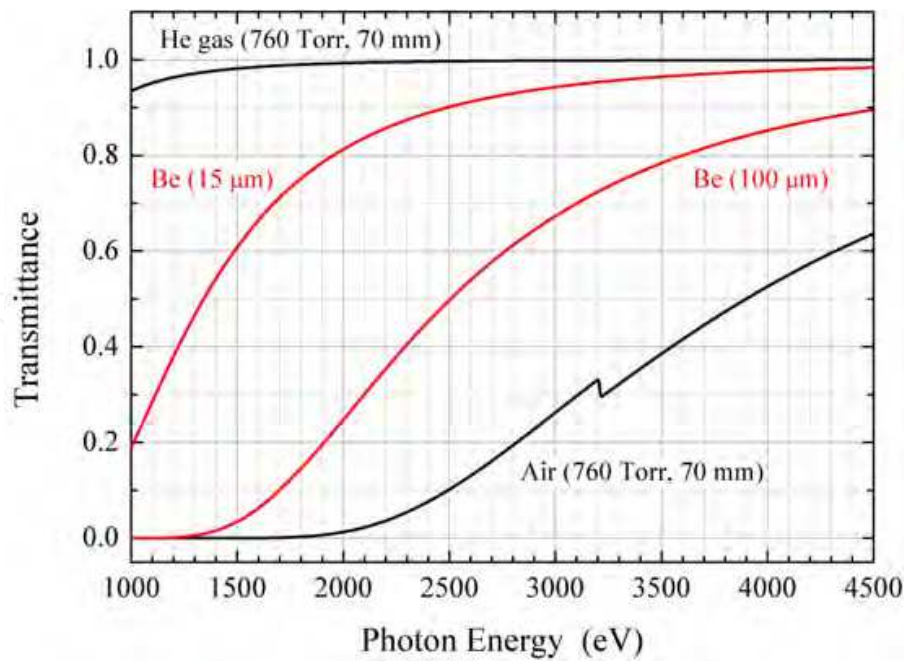


Fig. 3. Simulated transmittances of Air and He gas at 70 mm, which is the distance from the vacuum-tight window to the sample position in the AP sample chamber, and Be of 15 and 100 μm thickness. These simulations were used “X-ray Interaction with Matter Calculator”, the Center for X-ray Optics, Lawrence Berkeley National Laboratory, USA. Available from “http://henke.lbl.gov/optical_constants/”.

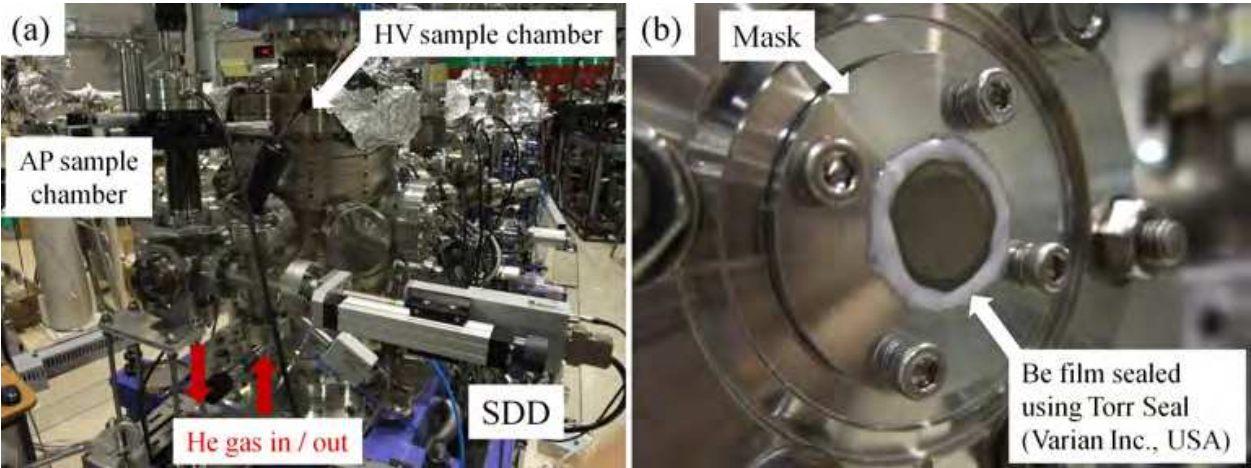


Fig. 4. Photos of the HV and AP sample chambers (a), and the vacuum-tight Be window (b).

Prior to the measurement, the AP chamber was filled with He gas to increase the transmittance of X-rays (see Fig. 3). It takes about 10 minutes to replace the air inside with He gas completely with the flow rate of $8.45 \times 10^{-1} \text{ Pa} \cdot \text{m}^3/\text{s}$ (500 sccm). The He gas flow rate was kept constant, typically at $3.38 \times 10^{-2} \text{ Pa} \cdot \text{m}^3/\text{s}$ (20 sccm) during measurements.

Now, the total EY (TEY) with specimen current, partial EY (PEY) using a PEY detector (as will hereinafter be described in detail), and partial FY (PFY) using a silicon drift detector (SDD) can be carried out in the HV sample chamber, while PFY can be carried out in the AP sample chamber.

For the performance test of BL-10, the photon flux was estimated from 1000 to 4500 eV using a Si PN photodiode (AXUV-SP2, International Radiation Detectors Inc., USA). In general, the photon flux Φ (photons/s) is given by the following formulae,

$$\Phi = \frac{i_p}{\eta e} \tag{1}$$

where i_p (A) is the short-circuit current of a photodiode. η is a quantum efficiency and e is a charge (A·s) [Saleh & Teich, 1991].

η is in the range ($0 \leq \eta \leq 1$), and is approximately proportional to the photon energy $h\nu$,

$$R = \frac{\eta e}{h\nu} \tag{2}$$

where R is called as ‘responsibility’, whose typical values are available from the WEB site of International Radiation Detectors Inc. (<http://www.ird-inc.com/>). The equation (3) is changed by,

$$\eta e = R h\nu \tag{3}$$

where ηe is called a device quantum yield. Substituting this equation (3) into the equation (1), we obtain the following,

$$\Phi = \frac{i_p}{R h\nu} \tag{4}$$

Fig. 5 shows the photon fluxes at the sample positions in the HV and AP sample chambers. All photon fluxes are normalized by the SR ring currents (200 mA). The difference of photon fluxes between in HV and AP is larger in the lower photon energy because of the transmittance for the Be window (see Fig. 3). However, the difference for the KTP crystal was relatively smaller than predicted that. This might be due to the radiation damage for the crystal, since the measurement was performed first in AP and later in HV sample chambers.

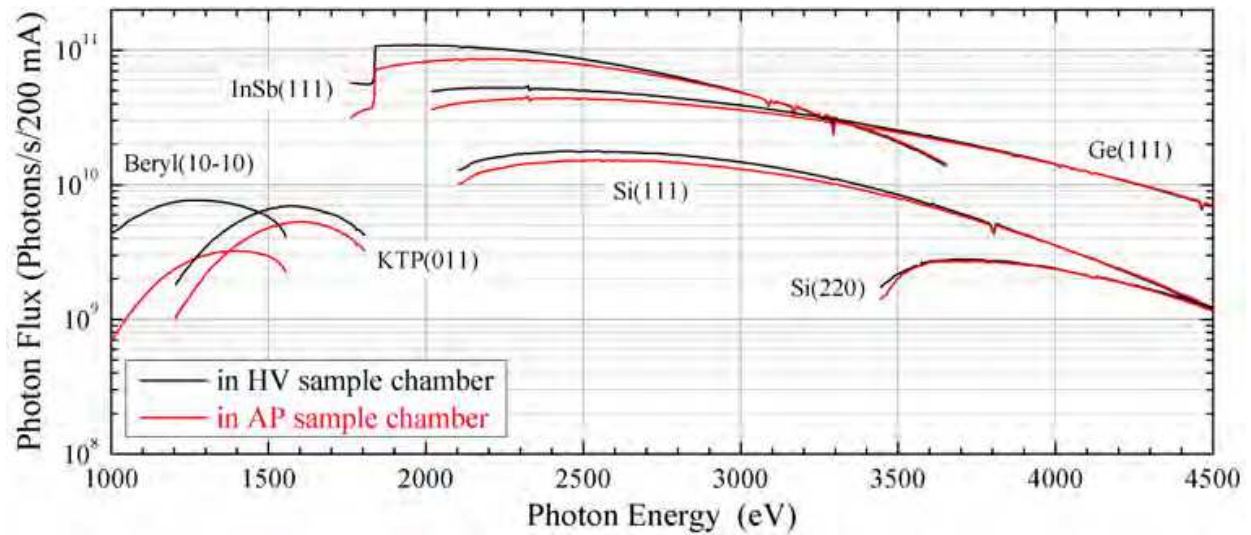


Fig. 5. Photon fluxes at the sample position in HV (black line) and AP (red line) sample chambers using each monochromatizing crystal.

To demonstrate the availability of the HV and AP chambers, XAFS measurements were carried out for anhydrous MgCl_2 and $\text{MgCl}_2 \cdot 6\text{H}_2\text{O}$. The crystal structures of MgCl_2 and $\text{MgCl}_2 \cdot 6\text{H}_2\text{O}$ are schematically shown in fig. 6. It is known that both samples are highly deliquescent. Since the local structures around Mg and Cl atoms are different from each other, it is expected different XAFS spectra are observed between MgCl_2 and $\text{MgCl}_2 \cdot 6\text{H}_2\text{O}$.

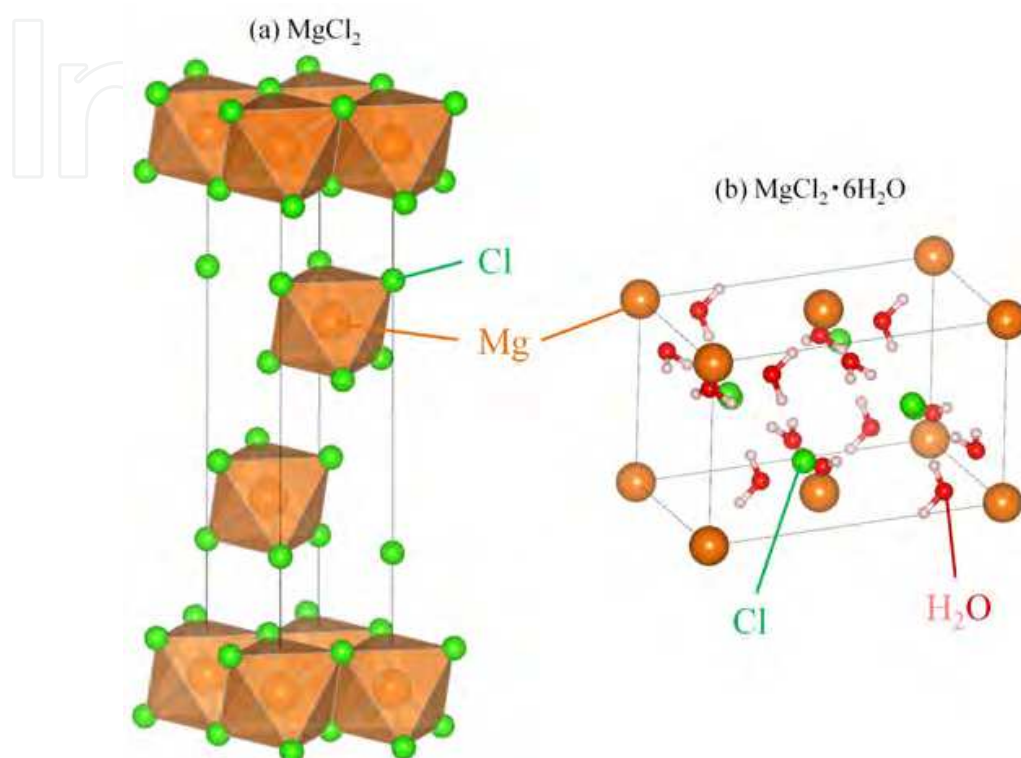


Fig. 6. Crystal structures of MgCl_2 (a) and $\text{MgCl}_2 \cdot 6\text{H}_2\text{O}$ (b) drawn by VESTA program [Momma & Izumi, 2008]. Each crystal information is referred from [Wyckoff, 1963] and [Agron et al., 1969].

Observed Mg and Cl K-edge X-ray absorption near edge structure (K-XANES) spectra which were measured both in HV and AP sample chambers are shown in Fig. 7. They are compared with theoretical XANES spectra simulated with the FEFF-8.4 program based on the real-space full multiple-scattering theory [Rehr et al., 2000]. Note that the white lines of PFY spectra in Fig. 7 are heavily suppressed compared with those of TEY spectra. This is due to the self-absorption effect in the PFY spectrum. In Mg K-XANES spectra of MgCl_2 (fig. 7 (a)), we can observe characteristic peaks; a white line at 1309.5 eV and a shoulder at 1311.5 eV. The spectral profile of TEY (HV) is well reproduced by the FEFF simulation. Those of PFY (HV), TEY (HV) are similar to that of PFY (AP), though the shoulder at 1311.5 eV is more enhanced in the spectrum of PFY (AP). In contrast, Mg K-XANES spectrum from $\text{MgCl}_2 \cdot 6\text{H}_2\text{O}$ in AP is distinctly different from those in HV, as shown in fig. 7 (b). The simulated spectrum is very similar to that of PFY (AP). This clearly indicates that the sample in vacuum is not $\text{MgCl}_2 \cdot 6\text{H}_2\text{O}$ anymore, but changed to anhydrous MgCl_2 , desorbing crystalline water molecules. In fact, the spectra from $\text{MgCl}_2 \cdot 6\text{H}_2\text{O}$ in HV (both PFY and TEY) are close to those of MgCl_2 in fig. 7 (a). Careful examination revealed that the spectrum from $\text{MgCl}_2 \cdot 6\text{H}_2\text{O}$ in HV (PFY) can be interpreted as a superposition of the spectra from

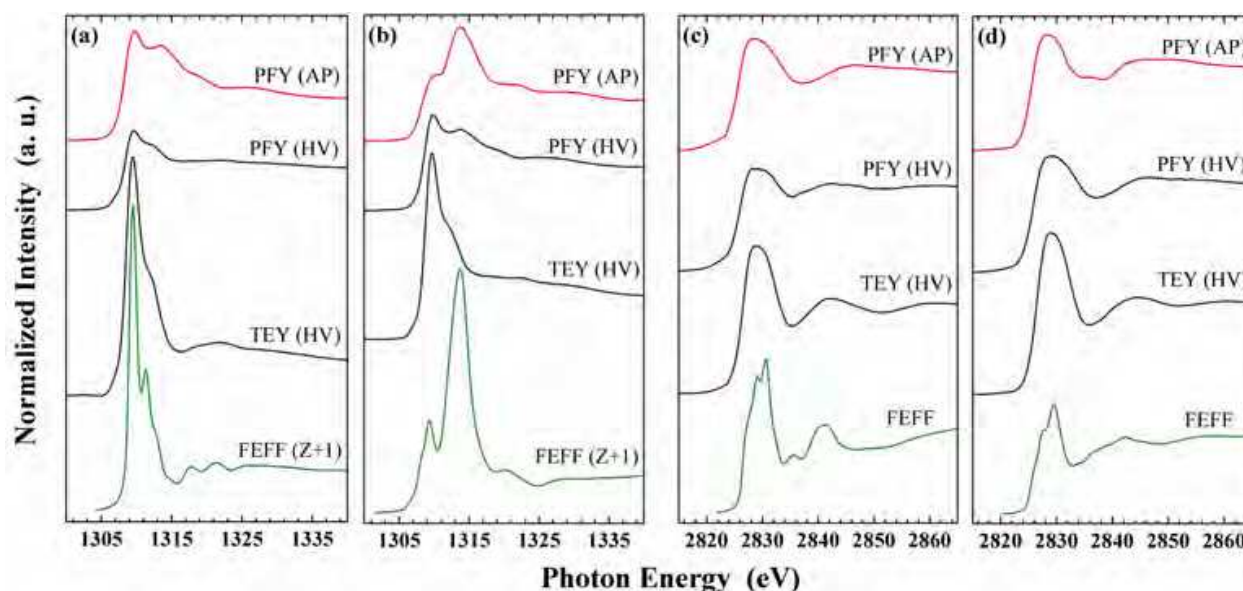


Fig. 7. Mg K-XANES spectra of MgCl_2 (a) and $\text{MgCl}_2 \cdot 6\text{H}_2\text{O}$ (b), and Cl K-XANES spectra of MgCl_2 (c) and $\text{MgCl}_2 \cdot 6\text{H}_2\text{O}$ (d) [Nakanishi et al., 2010]. Theoretical XANES spectrum with FEFF-8.4 is also shown in the bottom of each figure, where the Z+1 approach was used for (a) and (b) [Nakanishi & Ohta, 2009].

MgCl_2 and $\text{MgCl}_2 \cdot 6\text{H}_2\text{O}$. A part of $\text{MgCl}_2 \cdot 6\text{H}_2\text{O}$ might remain in bulk and be detected with the bulk-sensitive FY method. In fact, the spectrum was quickly measured in HV after evacuation.

As described above, an additional peak appears at 1313.5 eV in the spectrum from MgCl_2 of PFY (AP) in fig. 7 (a). This feature can be interpreted as the contribution from $\text{MgCl}_2 \cdot 6\text{H}_2\text{O}$, since highly deliquescent MgCl_2 adsorbed water during the sample preparation in air. This 'surface layer' is estimated to be about several μm orders. On the other hand, in the Cl K-XANES spectra from MgCl_2 and $\text{MgCl}_2 \cdot 6\text{H}_2\text{O}$, no significant difference was observed between the spectra measured in AP and HV, as shown in Fig. 7 (c), (d). This shows that hydrations occur exclusively around the Mg ions.

These results clearly demonstrate the necessity and the importance of XAFS measurements both in AP and HV in the soft X-ray region to obtain reliable spectra from hygroscopic and hydrated compounds.

2.3 Multiple Soft X-ray XAFS measurement system

The local structure and chemical composition of a sample surface are sometimes different from those of the bulk. Such differences play a critical role in functions of materials, such as catalytic activities, electronic properties of semiconductors, etc. Thus, there is a strong demand of depth-profiling techniques. As described in Introduction, the EY mode is generally used in the soft X-ray region, which is surface sensitive. The FY mode is sometimes used to probe bulk structures, although the intensity of the FY mode is one or two orders of magnitude lower than that of the EY mode. Combined use of these modes is known to be a powerful XAFS method for the depth profiling, as published so far [Yoon, et al., 2004].

There are some types in the EY mode. The TEY mode can be performed by only monitoring a specimen current without selecting electron energies using any detector or analyzer. Therefore it is adopted in many soft X-ray XAFS. The EY mode is surface sensitive compared with the FY mode, but especially in the higher-energy soft X-ray region, the sampling depth is not so small as expected [Frazer et al., 2003, Kasrai et al., 1996]. Others are needed to select electron energies with an electron detector or analyzer. The Auger electron yield (AEY) mode is the most surface sensitive and a high signal to background (S/B) ratio by collecting only Auger electrons using an electron analyzer [Gao et al., 2009]. However it is difficult sometimes to obtain a high signal to noise (S/N) ratio spectrum because of the low signal of detectable electrons for low concentration elements. The partial electron yield (PEY) mode collects only high energy electrons by filtering out secondary electrons and Auger electrons from other lower-energy absorption edges. The PEY mode is more surface-sensitive than the TEY mode, which is dominantly contributed by secondary electrons. A typical electron detector for the PEY mode is composed of two metal mesh grids for ground and retarding voltages, a chevron microchannel plates (MCPs) assembly with double MCPs and a metal collector [Stöhr, 1996]. In this detector, a suitable retarding voltage excludes low-energy electrons emerged from a deep bulk and extra signals from other lower-energy absorption edges. Hence, it enables us to obtain a spectrum with higher surface sensitivity and higher signal to background (S/B) ratio. The PEY method provides us with high quality spectra, and has been used in many XAFS studies, especially in the lower-energy soft X-ray region [Sako et al., 2005]. However, it should be noted that soft X-ray XAFS spectra by the PEY mode may sometimes cause a serious problem. It is well known that MCPs can detect not only electrons but also X-rays [Wiza, 1979]. When one uses the conventional MCP detector as an electron detector in soft X-ray XAFS experiments, one would get a spectrum deformed by unexpected inclusion of fluorescent X-rays.

In the lower-energy soft X-ray region below 1000 eV, the influence of fluorescent X-rays is very small and negligible, but it is not negligible in the higher-energy soft X-ray region, since the radiative core hole decay channel, i.e. fluorescent X-ray emission starts to open though the Auger decay process is still dominant [Krause, 1979]. Thus, we should be careful whether the PEY mode with an MCP detector provides reliable spectra or not.

A typical example is shown in Fig. 8 (a), which exhibits Si K-XANES spectra of a commercial thermally oxidized Si (SiO_2/Si) wafer with a 100 nm oxide overlayer (100 nm- SiO_2/Si wafer) taken with a conventional MCP detector. Observed TEY spectrum with specimen current is also shown for comparison, which gives the typical spectrum of SiO_2 . This result is reasonable, because the sampling depth of SiO_2/Si wafer by the TEY mode with specimen current is estimated to be about 70 nm, as reported by Kasrai et al. [Kasrai et al., 1996] and also confirmed by our experiments shown in fig. 11 (b). On the other hand, the XANES spectrum recorded by the conventional MCP detector at the retarding voltage of 0 V shows not only the feature of SiO_2 but also a weak feature of bulk Si at 1840 eV. In addition, by increasing the retarding voltage, the feature of bulk Si is more enhanced. In other words, increasing the retarding voltage appears to give bulk sensitive spectra. This result contradicts with a general tendency of the relation between a retarding voltage and sampling depth by the PEY method.

In order to explain this incongruous phenomenon, we show unnormalized spectra in fig. 8 (b). It shows how the retarding voltages change the spectra. As the retarding voltage

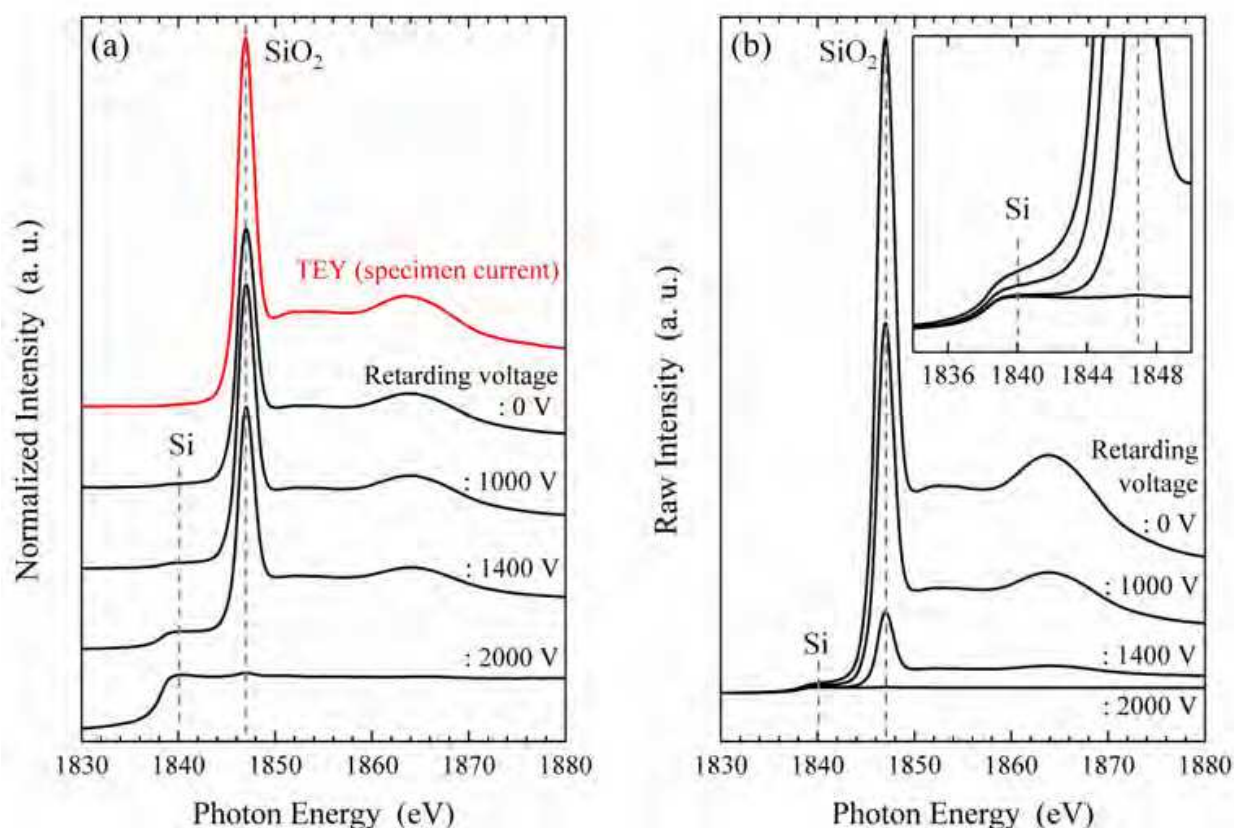


Fig. 8. Si K-XANES spectra of 100 nm-SiO₂/Si wafer obtained with the conventional MCP detector as a function of the retarding voltage. (a) Normalized spectra. The TEY spectrum with specimen current is also shown for comparison; (b) Unnormalized spectra.

increases, the peak intensity associated with SiO₂ decreases drastically, but the peak intensity at 1840 eV does not change at all (see inset of Fig. 8 (b)), even when the high retarding voltage (2000 V) is applied enough to eliminate all emitted electrons from the sample. It turns out that the origin of the peak at 1840 eV is fluorescent X-rays from bulk Si. This indicates that the XANES spectra by the conventional MCP detector at the retarding voltages of 0, 1000, and 1400 V are mixtures of both the PEY and total FY (TFY) spectra. By increasing the retarding voltage, number of electrons decreases, but that of fluorescent X-rays does not change. As the result, the TFY signal is relatively enhanced and the MCP detection gives a bulk sensitive spectrum apparently when the high retarding voltage is applied. In other words, the PEY spectrum is deformed by inclusion of unexpected TFY spectrum. Thus, in the soft X-ray region, one should use the conventional MCP detector as a PEY detector carefully, especially in the case that fluorescent X-rays from the bulk are not negligible.

Above results suggest that it is necessary to make the influence of fluorescent X-rays as small as possible for the PEY mode. Bearing it in mind, we designed and fabricated a new PEY detector using a MCP assembly. The schematics and photograph are shown in Fig. 9. There are two major modifications from the conventional MCP detector. The first is to bend the trajectory of emitted electrons from a sample so as to collect only electrons in the MCPs.

For this purpose, three cylindrical austenitic stainless steel (ASS) grids, whose the transmission rate is about 77.8 %, were used. The bending voltage of 3000 V was applied between

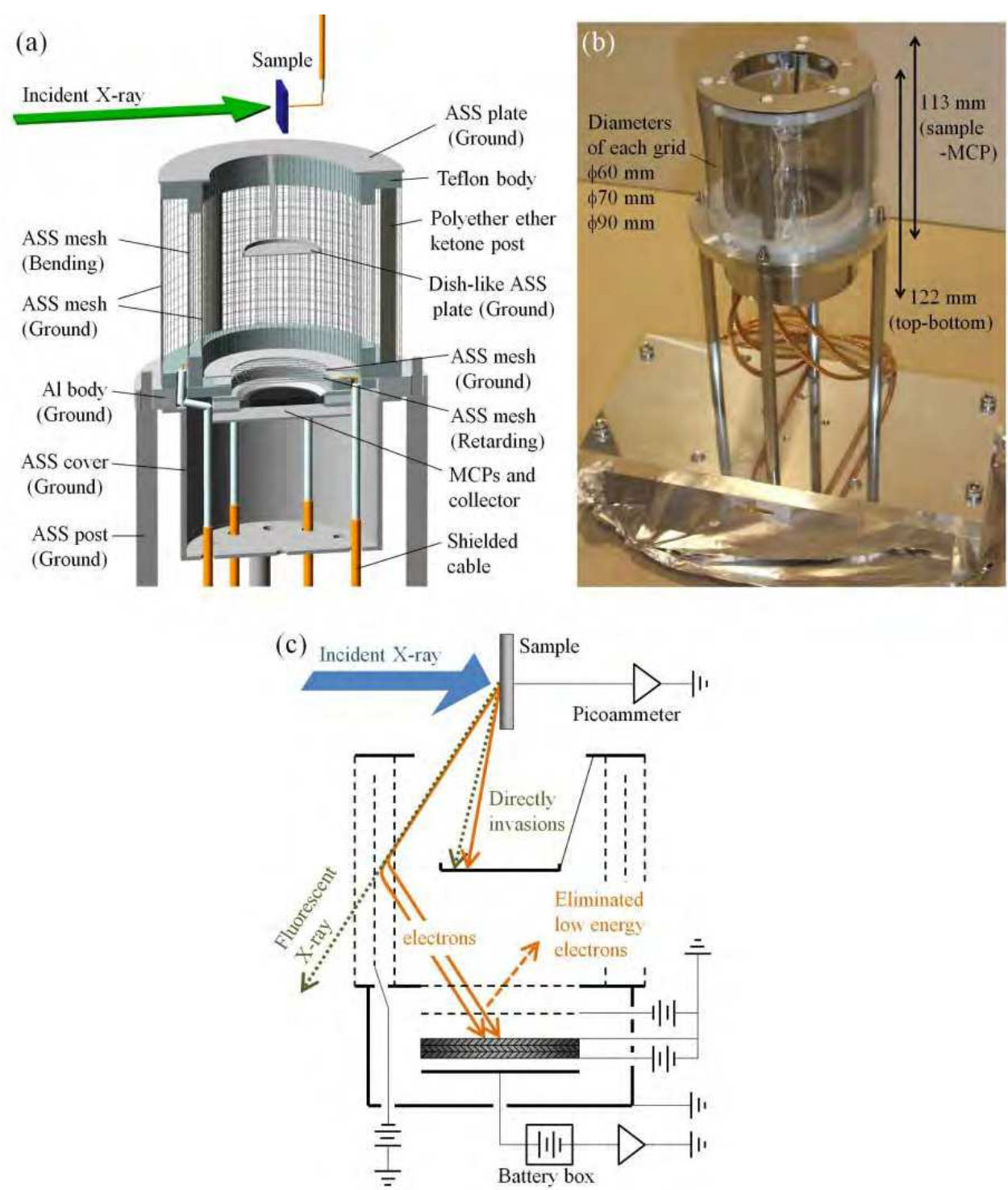


Fig. 9. Newly-developed PEY detector for the soft X-ray region [Nakanihshi & Ohta, In press]. (a) The experimental layout. The cross section of the detector is shown for the details; (b) Photograph; (c) The operating principle for the PEY measurement.

the inner and the intermediate grids, and the outer grid works to prevent from a leak voltage. The second is to place the dish-like ASS plate between a sample and MCPs so as to avoid direct invasions of fluorescent X-rays (and electrons) into MCPs. These two modifications make the PEY measurements work effectively in the higher-energy soft X-ray

region as same as the conventional MCP detector in the lower-energy soft X-ray region. For the detector, a Z-stack MCP assembly, whose MCPs have the diameter of 25 mm and the aspect ratio of 60:1 (Long-Life MCPs, Photonis USA Inc., USA) was used.

To examine the performance of the detector, we prepared a Si wafer etched in 1.0 % aqueous solution of HF (HF-Si wafer) and several SiO₂/Si wafers with different oxide overlayer thickness by heating at 950 K in an electric furnace. The oxide overlayer thickness of each sample was controlled by the heating time and estimated by ellipsometric measurements (λ = 633 nm), in which the refractive index was fixed to 1.457 [Malitson, 1965]. The photon energy was calibrated by setting the first peak of the first derivative in the Si K-edge XAFS (K-XAFS) spectrum of a Si wafer to 1839 eV [Nakanishi, 2009]. PFY spectra were using the SDD with the selected energy window for Si-K α X-rays.

Fig. 10 (a) shows observed Si K-edge PEY spectra of 25.3 nm-SiO₂/Si wafer as a function of the retarding voltage, together with the TEY and PFY spectra for comparison. Compared with the TEY spectrum, the PEY spectrum at the retarding voltage of 0 V is slightly more surface sensitive. This is because the detector collects electrons emitted in the oblique angle, as shown in Fig. 9 (c).

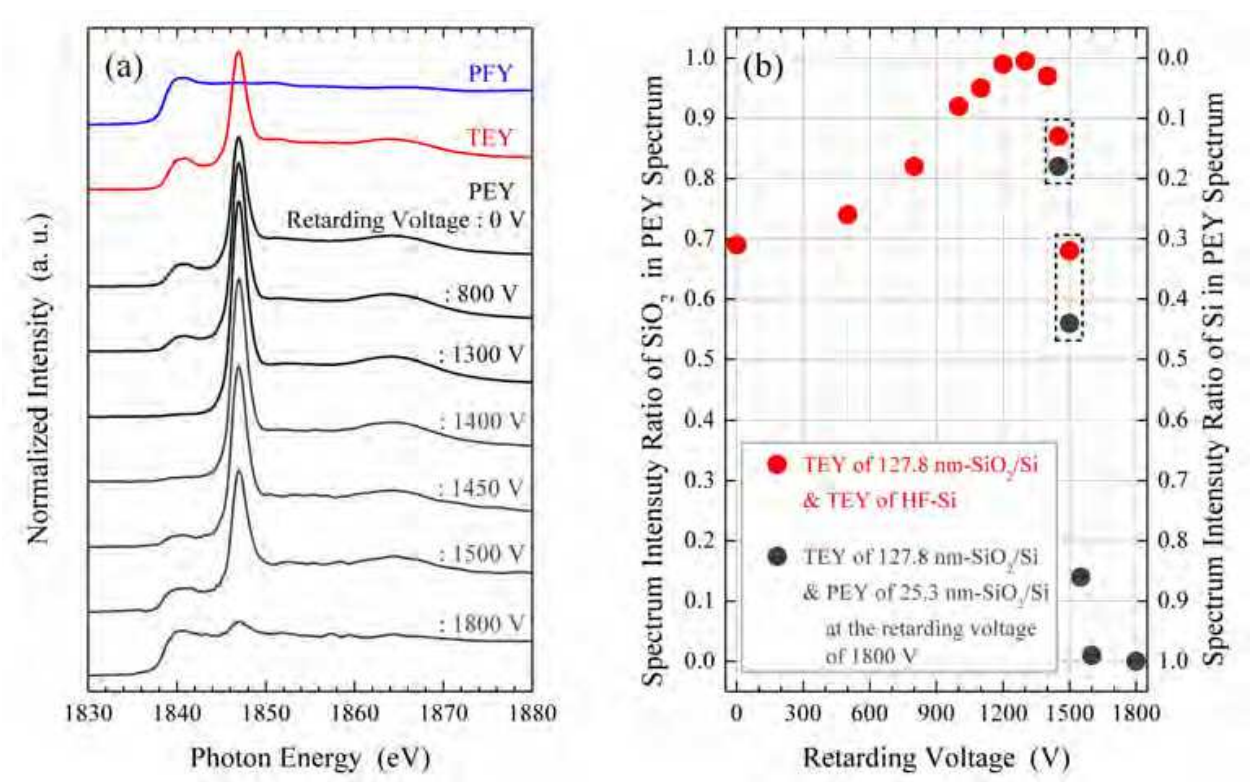


Fig. 10. (a) Observed Si K-XANES spectra of 25.3 nm-SiO₂/Si using the PEY detector at several retarding voltages. The PFY spectrum using the SDD, and TEY spectrum with specimen current are also shown for comparison. The self-absorption effect of the PFY spectrum is not corrected; (b) The distribution of SiO₂ and Si intensity ratio in PEY spectra of 25.3 nm-SiO₂/Si wafer as a function of the retarding voltage.

Fig. 10 (b) shows how surface SiO₂ and bulk Si contribute to each PEY spectrum as a function of the retarding voltage. Spectrum intensity ratios in each PEY spectrum are

analyzed as the superposition of these two spectra: SiO₂ and bulk Si. Here, we adopt the TEY spectrum of 127.8 nm-SiO₂/Si wafer to stand for SiO₂, and the TEY spectrum of HF-Si wafer to stand for bulk Si. Note the PEY spectrum of 25.3 nm-SiO₂/Si at the retarding voltage of 1800 V is also used as the spectrum of bulk Si for the analysis, when the retarding voltage of PEY spectra is higher than 1400 V. As the retarding voltage increases from 0 to 1300 V, the SiO₂ intensity increases and the Si intensity decreases. This is the reasonable tendency of the PEY measurements unlike that of the conventional MCP detector in the previous section. However, as the retarding voltage increases further from 1300 to 1800 V, the SiO₂ intensity decreases dramatically and the bulk Si intensity increases, relatively. At the retarding voltage of 1800 V, we could obtain a PEY spectrum which was close to that of bulk Si, even though Si KLL Auger electrons could not reach the MCP at the voltage.

About the above phenomenon, we think the following reason. A part of fluorescent X-rays or electrons emitted from the sample were scattered on the surface of parts of the detector, then they are entered the MCP on unexpected trajectories. In addition, A part of fluorescent X-rays and electrons excited atoms in parts of the detector as a probe, then generated newly fluorescent X-rays and electrons also entered the MCP on unexpected trajectories. Here, most of newly-generated electrons were excluded by the retarding voltage, but electrons emitted from the intermediate grid for bending electrons of the detector could reach the MCP because they were accelerated by the voltage between the intermediate grid and the inner grid. These effects could be neglected when the retarding voltage was below 1300 V, since the intensities of intrinsic electrons are dominant. Above 1300 V, These effects could not be neglected, since the intensity of intrinsic electrons suddenly dropped. However, the MCP gain had to be enhanced by increasing the MCP voltage from 2400 V to 3200 V in order to get spectra when the retarding voltage was above 1300 V. These indicate that retarding voltages above 1300 V are not suitable for the PEY detection at Si K-XAFS measurements using this detector.

It was determined to be 1300 V for Si K-edge from the above results. Here, the S/B ratio was confirmed for the PEY spectrum with the optimum retarding voltage. At the photon energy of 2000 eV, the S/B ratio of the PEY spectrum of 25.3 nm-SiO₂/Si wafer was 4.95. This was superior to that of the PEY spectrum without retarding voltage (3.40) and the TEY spectrum with specimen current (1.64).

Then, we estimated the sampling depth of the PEY detection. Fig. 11 (a) shows the PEY spectra of SiO₂/Si as a function of the oxide overlayer thickness at the retarding voltage of 1300 V. For comparison, the result of TEY spectra is also shown in fig. 11 (b). As the oxide overlayer thickness increases, the spectrum intensity ratio of SiO₂ increases and saturates in fig. 11 (c). From this spectrum intensity ratio profile, the sampling depth at Si K-edge of the PEY was estimated to be about 30 nm in the SiO₂/Si system. This is less than half of that of the TEY.

Combining the PEY detector (PEY) with the specimen current (TEY) and the SDD (PFY), we can get multiple information about sampling depths; surface, interface and bulk. It is greatly valuable and efficient to obtain the depth profile of an unknown sample. Fig. 12 shows the detection system and demonstrative Si K-XANES spectra of 25.3 nm-SiO₂/Si. The three spectra were observed with different spectral features depending on each sampling depth (shown in fig. 12 (b)). This simultaneous soft X-ray XAFS system is not only useful to obtain

detailed information about a sample but also important for XAFS users with limited available beam time in a synchrotron radiation facility.

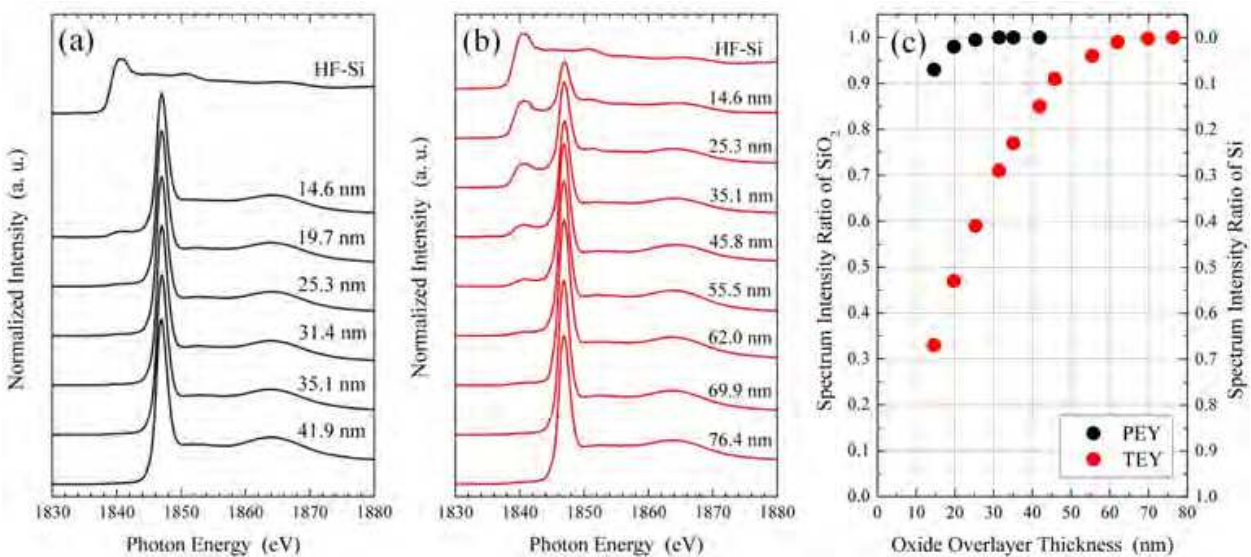


Fig. 11. Si K-XANES spectra of several SiO₂/Si samples with the PEY mode (a) and the TEY mode (b) as a function of the oxide overlayer thickness; (c) The distribution of SiO₂ and Si intensity ratio in PEY and TEY spectra of several SiO₂/Si samples as a function of the oxide overlayer thickness.

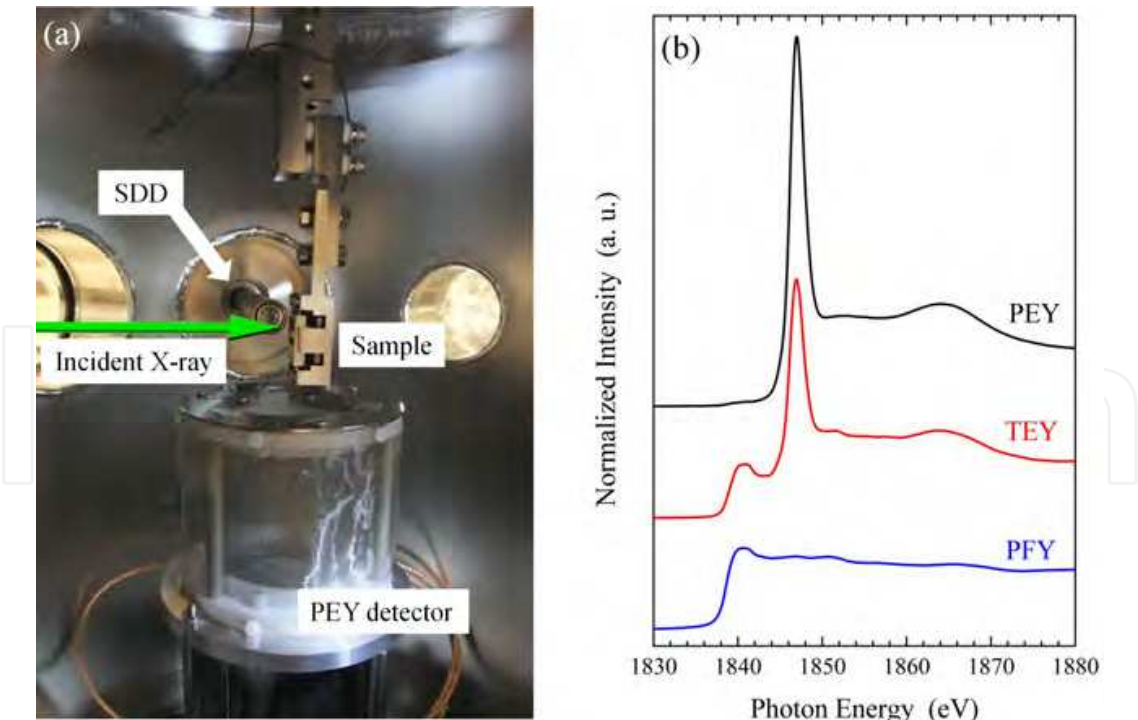


Fig. 12. Multiple soft X-ray XAFS measurement system. (a) Photograph of the experimental setup in the HV sample chamber; (b) Si K-XANES spectra of 25.3 nm-SiO₂/Si detected by the PEY detector at the retarding voltage of 1300 V (PEY), the specimen current (TEY), and the SDD (PFY). The self-absorption effect is not corrected in the PFY spectrum.

2.4 Transfer vessel system for anaerobic samples

We sometimes encounter a problem to measure anaerobic samples, such as highly deliquescent materials, e.g. MgCl_2 and $\text{MgCl}_2 \cdot 6\text{H}_2\text{O}$ as described in section 2.2 and highly hydrolytic materials, e.g. Li-ion battery (LIB) materials. One of the difficulties is how to carry such a sample from a laboratory to an SR facility and how to set it up in an XAFS equipment without exposing to air. An aluminum-laminated bag is often used to seal the sample with a high-purity Ar gas in a glove box. It is possible to measure the sample in the hard X-ray region, but is impossible in the soft X-ray region because of the low transmittance for an aluminum-laminated bag. In order to solve the problem, we developed a compact transfer vessel system (see fig. 13) [Nakanishi & Ohta, 2010].

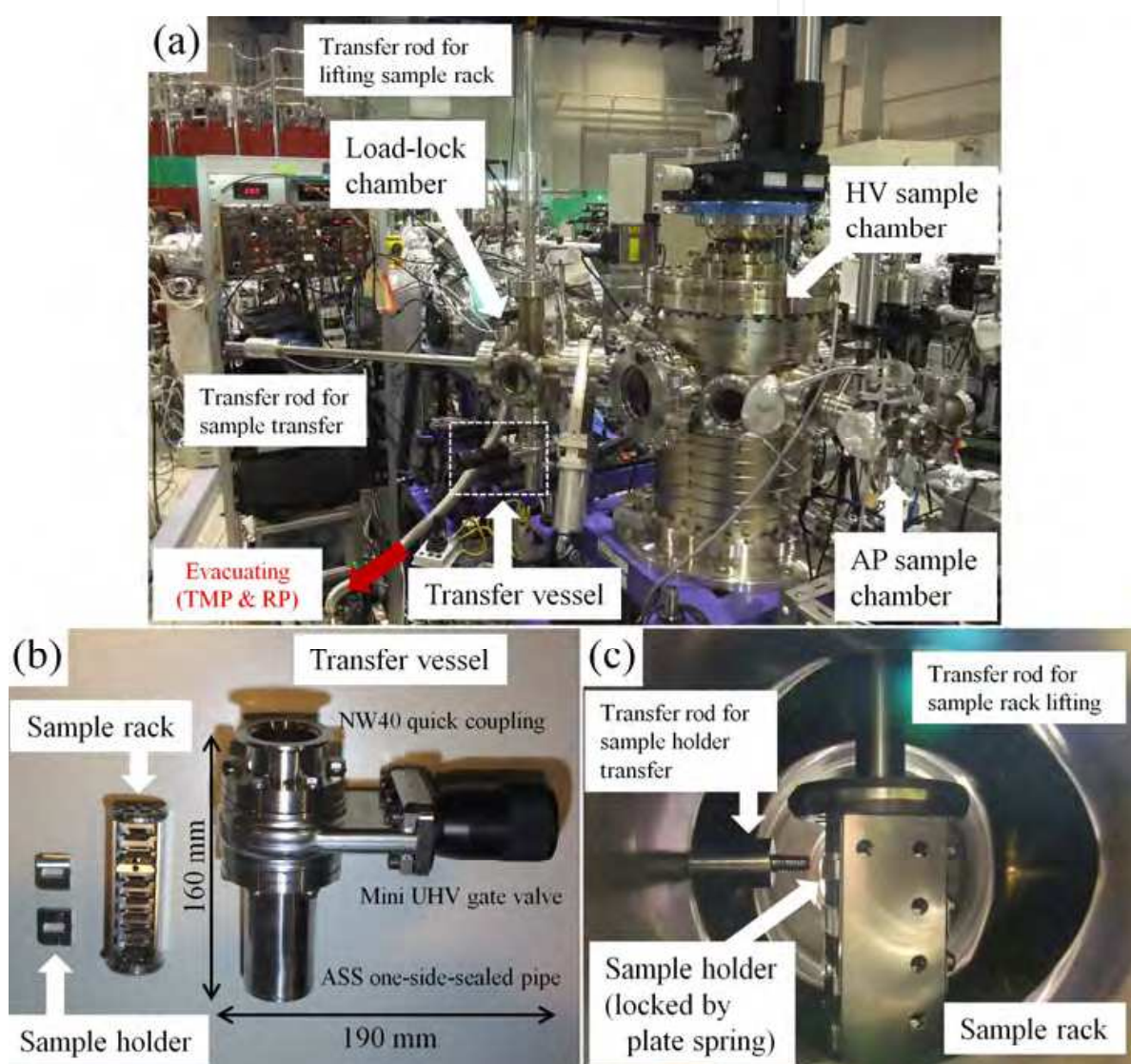


Fig. 13. Photos of developed transfer vessel system. (a) The load-lock chamber and the HV sample chamber; (b) the transfer vessel, sample rack and sample holders; (c) inside of the load-lock chamber.

It consists of an ICF70 UHV gate valve (Mini UHV gate valve, VAT Vacuumvalves AG, Switzerland), an ASS one-side-sealed pipe, an ICF70-NW40 flange. The vessel is compact

enough to be handled in a commercial glove box. Normally two samples are mounted on the sample holder with carbon tapes. Eight sample holders can be set in the sample rack. After the sample rack with sample holders is loaded into the vessel, the UHV gate valve of the vessel is closed tightly together with a high-purity Ar gas in a glove box. Then the vessel is taken out from the glove box. The sealed vessel can be carried to the SR center and is connected to the load-lock chamber, as shown in Fig. 13 (a). After evacuating the chamber using a turbomolecular pump (TMP) and rotary pump (RP), the gate valve of the vessel is opened. The rack with sample holders is pulled out from the vessel and lifted to the transfer position in the load-lock chamber by the transfer rod. Each sample holder in the rack is transferred and loaded into the HV sample chamber for XAFS measurements. The HV sample chamber and load-lock chamber are kept in HV until all XAFS measurements are over.

For evaluation of the sealing capacity of the vessel, we monitored dew points in the vessel. The transfer vessel with a dew point temperature sensor probe (Moisture Target Series 5, GE Measurement & Control Solutions, USA) was prepared (see fig.14 (a)) and monitored dew point temperatures enclosed sixteen LIB electrode samples, LiCoO_2 powders with acetylene black and poly-vinylidene difluoride (PVDF) coated on Al films, with an Ar gas in a glove box (see fig. 14 (b)). The sealed vessel was ejected from the glove box as soon as closing the valve. It is shown that the dew point temperature increased gradually. After 24 hours, the dew point temperature is about -80°C . This is the sufficient value to carry LIB samples or others prepared in a glove box without changing the condition.

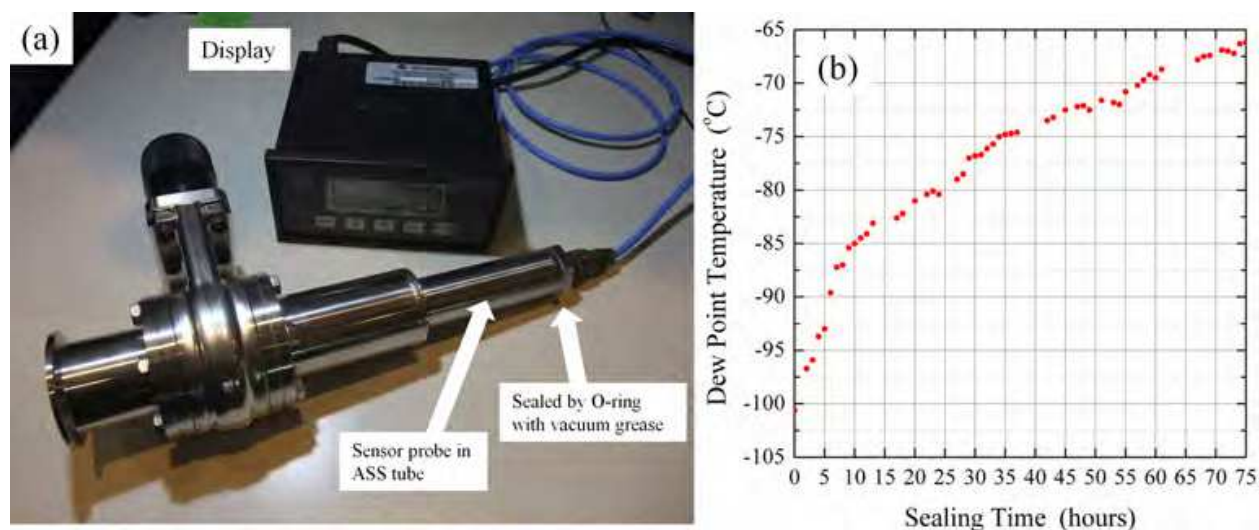


Fig. 14. (a) Photograph of the developed transfer vessel with a dew point temperature sensor probe; (b) Monitored dew point temperature plots in the sealed vessel with LIB samples.

XAFS measurements of LiPF_6 known as an LIB electrolyte material were demonstrated. Fig. 15 (b) shows P K-XANES spectra of LiPF_6 powders carried by the sealed vessel without air exposure and air exposure for 1 day by the TEY and PFY modes. For comparison, the simulated spectrum of LiPF_6 , the experimental spectra of Li_3PO_4 powder and H_3PO_4 solution are also shown in fig. 15 (b). Experimental spectra of LiPF_6 without air exposure are in good agreement between the TEY and PFY spectrum, and are also reproduced by simulated spectrum. However, the small difference at the energy position of the pre-edge peak is

confirmed between the TEY and PFY spectrum. Meanwhile both experimental spectra of LiPF_6 with air exposure have similar features to Li_3PO_4 and H_3PO_4 , such as the white line at 2152.9 eV (black dashed line) and the broad peak around 2170 eV. This indicates most local structures of P atoms in LiPF_6 changed the octahedral coordination with F atoms shown in fig. 15 (a) into the tetrahedral coordination with O atoms (i.e. phosphates). Hence we identified surface P atoms in LiPF_6 without air exposure has been also changed into phosphates, because the energy position of the pre-edge peak of the TEY spectrum closes to that of the white line of phosphates. We think that only the surface of LiPF_6 samples has been changed by negligible moisture in a glove box over the course of several weeks. About LiPF_6 with air exposure, both the TEY and PFY spectrum shape are very similar to that of Li_3PO_4 , but the shoulder peak at 2154.5 eV (red dashed line) can be seen only spectra of LiPF_6 with air exposure. This origin is not clear yet, but may originate from POF_3 , $\text{POF}_2(\text{OH})$ or other materials generated by hydrolyzed LiPF_6 [Kawamura et al., 2006].

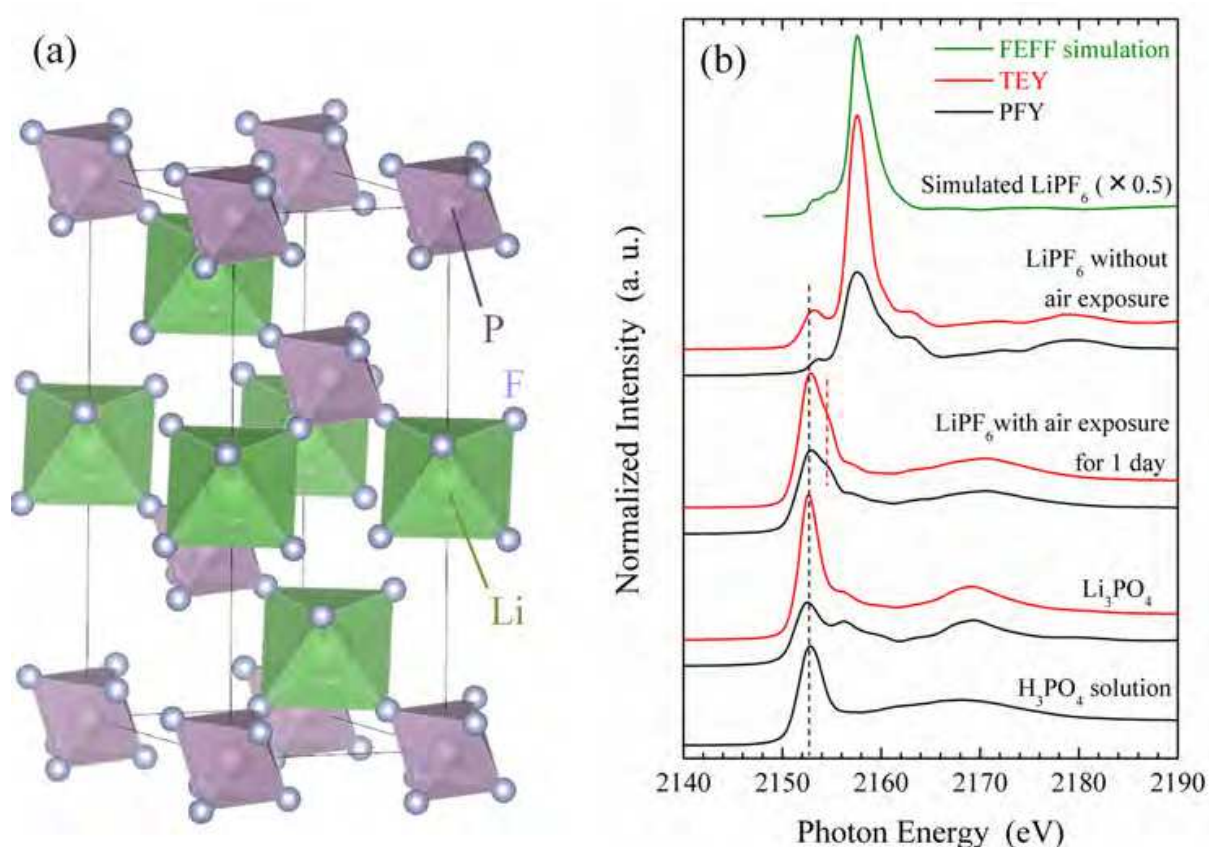


Fig. 15. (a) Crystal structure of LiPF_6 drawn by VESTA program [Momma & Izumi, 2008]. The crystal information is referred by [Röhr & Kniep, 1994]; (b) Simulated spectra of LiPF_6 by FEFF program and experimental P K-XANES spectra of LiPF_6 with and without air exposure. TEY spectra of Li_3PO_4 and H_3PO_4 are also shown as a reference sample. The self-absorption effect is not corrected in PFY spectra.

From these results, it is clearly indicated the efficiency of the vessel to carry the highly hydrolytic materials without changing the chemical condition. This transfer vessel system is using in many case, and especially in LIB materials, the system is absolutely essential.

3. Conclusion

We developed the unique and efficient soft X-ray XAFS measurement system at BL-10 of the SR center, Ritsumeikan University. As well as being able to accept stable solid samples in the HV sample chamber, hygroscopic and hydrated compounds, which are changed the condition in vacuum, and liquid samples are also able to accept in the AP chamber with the vacuum-tight window of a thin Be foil and in He gas atmosphere. In the HV chamber, a multiple measurement combined with the TEY, PEY, and PFY methods can give us the depth profile of samples. This is very useful for chemical analysis of practical samples. In addition, the transfer vessel system is an efficient tool for carrying anaerobic samples without changing chemical conditions. These setups will satisfy with many demands for various sample conditions. We hope that this XAFS system will be used by many users and stimulate further soft X-ray XAFS studies.

4. Acknowledgment

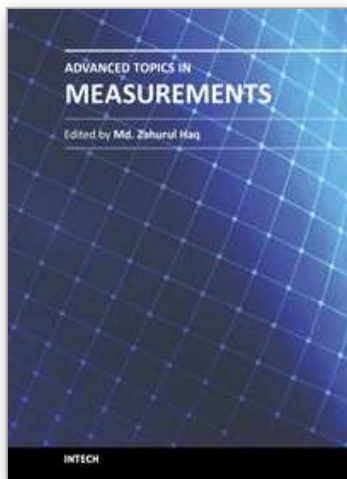
The authors acknowledge Prof. Shinya Yagi (Nagoya University, Japan) for his invaluable advices in development of the atmospheric-pressure sample chamber, Dr. Yasuhiro Abe (Ritsumeikan University, Japan) for his technical support in ellipsometric measurements, Dr. Masatsugu Oishi (Kyoto University, Japan), Mr. Takahiro Kakei (Kyoto University, Japan), Dr. Tomonari Takeuchi (National Institute of Advanced Industrial Science and Technology, Japan) and Dr. Hiroyuki Kageyama (National Institute of Advanced Industrial Science and Technology, Japan) for their assistances in providing samples to evaluate the transfer vessel.

These works were partially supported by Nanotechnology Network (Nanonet) Project from Ministry of Education, Culture, Sports, Science and Technology (MEXT) in Japan, and by Research and Development Initiative for Scientific Innovation of New Generation Batteries (RISING) project from New Energy and Industrial Technology Development Organization (NEDO) in Japan.

5. References

- Agron, P. A. & Busing, W. R. (1969). A neutron diffraction study of magnesium chloride hexahydrate, *Acta Cryst. A*, Vol. 25, pp. 118-119.
- Frazer, B. H.; Gilbert, B.; Sonderegger, B. R. & G. D. Stasio, (2003), The probing depth of total electron yield in the sub-keV range : TEY-XAS and X-PEEM, *Surf. Sci.*, Vol. 537, pp. 161-167.
- Gao, X.; Chen, S.; Liu, T.; Chen, W.; Wee, A. T. S.; Nomoto, T.; Yagi, S.; Soda, K. & Yuhara, J. (2009). Si clusters on reconstructed SiC (0001) revealed by surface extended x-ray absorption fine structure, *App. Phys. Lett.*, Vol. 95, pp. 144102-144105.
- Golovchenko, J. A.; Levesque, R. A. & Cowan, P. L. (1981). X-ray monochromator system for use with synchrotron radiation sources, *Rev. Sci. Instrum.*, Vol. 52, pp.509-516.
- Handa, K.; Sakai, I.; Izuhara, O.; Iwasaki, H.; Yoshimura, Y.; Masui, S. & Murata, T.(1999). Soft X-ray XAFS Beamline for Advanced Materials Research at Compact Superconducting Ring, *Jpn. J. Appl. Phys.*, Vol. 38, Suppl. 38-1, pp. 654-657.

- Iwasaki, H.; Nakayama, Y.; Ozutsumi, K.; Yamamoto, Y.; Tokunaga, Y.; Saisho, H.; Matsubara, T. & Ikeda, S. (1998). Compact Superconducting Ring at Ritsumeikan University, *J. Synchro. Rad.*, Vol. 5, pp. 1162-1165.
- Kasrai, M.; Lennard, W. N.; Brunner, R. W.; Bancroft, G. M.; Bardwell, J. A. & Tan, K. H. (1996). Sampling depth of total electron and fluorescence measurements in Si L- and K-edge absorption spectroscopy, *Appl. Surf. Sci.*, Vol. 99, pp. 303-312.
- Kawamura, T.; Okada, S. & Yamaki, J. (2006). Decomposition reaction of LiPF_6 based electrolytes for lithium ion cells, *J. Power Sources*, Vol. 156, pp. 547-554.
- Krause, M. O. (1979). Atomic Radiative and Radiationless Yields for K and L Shells, *J. Phys. Chem. Ref. Data*, Vol. 8, pp. 307-327.
- Lai, B. & Cerrina, F. (2002). SHADOW: A synchrotron radiation ray tracing program, *Nucl. Instrum. Methods A*, Vol. 246, pp. 337-341.
- Malitson, I. H. (1965). Interspecimen Comparison of the Refractive Index of Fused Silica, *J. Opt. Soc. Am.*, Vol. 55, pp. 1205-1208.
- Momma, K. & Izumi, F. (2008). VESTA: a three-dimensional visualization system for electronic and structural analysis, *J. Appl. Crystallogr.*, Vol. 41, pp. 653-658.
- Nakanishi, K. & Ohta, T. (2009). Verification of the FEFF simulations to K-edge XANES spectra of the third row elements, *J. Phys. : Condens. Matter*, Vol. 21, pp. 104214-104219.
- Nakanishi, K. & Ohta, T. (In press). Improvement of the Detection System in the Soft X-ray Absorption Spectroscopy, *Surf. Interface Anal.*
- Nakanishi, K.; Yagi, S. & Ohta, T. (2010). Development of a XAFS Measurement System in the Soft X-ray Region for Various Sample Conditions (in Japanese), *IEEJ Trans. EIS*, Vol. 130, pp.1762-1767.
- Nakanishi, K.; Yagi, S. & Ohta, T. (2010). XAFS Measurements under Atmospheric Pressure in the Soft X-ray Region, *AIP Conf. Proc.*, Vol. 1234, pp. 931-934.
- Ohta, T. (Ed.), (2002). *X-ray Absorption Spectroscopy* (in Japanese), Industrial Publishing & Consulting, Inc., Japan, ISBN: 978-4901493215.
- Rehr, J. J. & Albers, R. C. (2000). Theoretical approaches to x-ray absorption fine structure, *Rev. Mod. Phys.* Vol. 72, pp. 621-654.
- Röhr, C. & Kniep, R. (1994). The crystal structures of $\text{Li}(\text{PF}_6)$ and $\text{Li}(\text{AsF}_6)$: on the crystal chemistry of compounds $\text{A}(\text{E}^{\text{V}}\text{F}_6)$, *Zeitschrift für Naturforschung. B, A journal of chemical sciences*, Vol. 49, pp. 650-654.
- Sako, E. O.; Kondoh, H.; Nakai, I.; Nambu, A.; Nakamura, T. & Ohta, T. (2005). Reactive adsorption of thiophene on Au(111) from solution, *Chem. Phys. Lett.*, Vol. 413, pp. 267-271.
- Saleh, B. E. A. & Teich, M. C. (1991). *Fundamentals of Photonics*, Wiley Series in Pure and Applied Optics, Wiley-Interscience, ISBN 978-0471358329.
- Stöhr, J. (1996). *NEXAFS Spectroscopy*, Springer Series in Surface Science, Vol. 25, Springer-Verlag, Berlin, ISBN: 978-3642081132.
- Welnak, C.; Chen, G. J. & Cerrina, F. (1994). SHADOW: A synchrotron radiation and X-ray optics simulation tool, *Nucl. Instrum. Methods A*, Vol. 347, pp. 344-347.
- Wiza, J. L. (1979). Microchannel plate detectors, *Nucl. Instr. and Meth.*, Vol. 162, p. 587-601.
- Wyckoff, R. W. G. (1963). *Crystal Structures*, Vol. 1, Interscience Publishers, New York, ISBN: 978-0471968696.
- Yoon, W-S.; Balasubramanian, M.; Yang, X-Q.; Fu, Z.; Fischer, D.A. & McBreen, J. (2004). Soft X-Ray Absorption Spectroscopic Study of a $\text{LiNi}_{0.5}\text{Mn}_{0.5}\text{O}_2$ Cathode during Charge, *J. Electrochem. Soc.*, Vol. 151, pp. A246-A251.



Advanced Topics in Measurements

Edited by Prof. Zahurul Haq

ISBN 978-953-51-0128-4

Hard cover, 400 pages

Publisher InTech

Published online 07, March, 2012

Published in print edition March, 2012

Measurement is a multidisciplinary experimental science. Measurement systems synergistically blend science, engineering and statistical methods to provide fundamental data for research, design and development, control of processes and operations, and facilitate safe and economic performance of systems. In recent years, measuring techniques have expanded rapidly and gained maturity, through extensive research activities and hardware advancements. With individual chapters authored by eminent professionals in their respective topics, Advanced Topics in Measurements attempts to provide a comprehensive presentation and in-depth guidance on some of the key applied and advanced topics in measurements for scientists, engineers and educators.

How to reference

In order to correctly reference this scholarly work, feel free to copy and paste the following:

Koji Nakanishi and Toshiaki Ohta (2012). XAFS Measurement System in the Soft X-ray Region for Various Sample Conditions and Multipurpose Measurements, Advanced Topics in Measurements, Prof. Zahurul Haq (Ed.), ISBN: 978-953-51-0128-4, InTech, Available from: <http://www.intechopen.com/books/advanced-topics-in-measurements/xafs-measurement-system-in-the-soft-x-ray-region-for-various-sample-conditions-and-multipurpose-meas>

INTECH
open science | open minds

InTech Europe

University Campus STeP Ri
Slavka Krautzeka 83/A
51000 Rijeka, Croatia
Phone: +385 (51) 770 447
Fax: +385 (51) 686 166
www.intechopen.com

InTech China

Unit 405, Office Block, Hotel Equatorial Shanghai
No.65, Yan An Road (West), Shanghai, 200040, China
中国上海市延安西路65号上海国际贵都大饭店办公楼405单元
Phone: +86-21-62489820
Fax: +86-21-62489821

© 2012 The Author(s). Licensee IntechOpen. This is an open access article distributed under the terms of the [Creative Commons Attribution 3.0 License](https://creativecommons.org/licenses/by/3.0/), which permits unrestricted use, distribution, and reproduction in any medium, provided the original work is properly cited.

IntechOpen

IntechOpen